Biophysical Journal
Article

Biophysical Society

Cholesterol Increases the Openness of SNARE-Mediated Flickering Fusion Pores

Benjamin S. Stratton,[1] Jason M. Warner,[1] Zhenyong Wu,[2,3] Joerg Nikolaus,[2,3] George Wei,[1] Emma Wagnon,[1] David Baddeley,[3,4] Erdem Karatekin,[2,3,5,6,*] and Ben O'Shaughnessy[1,*]

[1]Department of Chemical Engineering, Columbia University, New York, New York; [2]Department of Cellular and Molecular Physiology, Yale University, School of Medicine, New Haven, Connecticut; [3]Nanobiology Institute, Yale University, West Haven, Connecticut; [4]Department of Cell Biology and [5]Department of Molecular Biophysics and Biochemistry, Yale University, New Haven, Connecticut; and [6]Laboratoire de Neurophotonique, Université Paris Descartes, Centre National de la Recherche Scientifique (CNRS) UMR8250, Paris, France

ABSTRACT Flickering of fusion pores during exocytotic release of hormones and neurotransmitters is well documented, but without assays that use biochemically defined components and measure single-pore dynamics, the mechanisms remain poorly understood. We used total internal reflection fluorescence microscopy to quantify fusion-pore dynamics in vitro and to separate the roles of soluble *N*-ethylmaleimide-sensitive factor attachment protein receptor (SNARE) proteins and lipid bilayer properties. When small unilamellar vesicles bearing neuronal v-SNAREs fused with planar bilayers reconstituted with cognate t-SNARES, lipid and soluble cargo transfer rates were severely reduced, suggesting that pores flickered. From the lipid release times we computed pore openness, the fraction of time the pore is open, which increased dramatically with cholesterol. For most lipid compositions tested, SNARE-mediated and nonspecifically nucleated pores had similar openness, suggesting that pore flickering was controlled by lipid bilayer properties. However, with physiological cholesterol levels, SNAREs substantially increased the fraction of fully open pores and fusion was so accelerated that there was insufficient time to recruit t-SNAREs to the fusion site, consistent with t-SNAREs being preclustered by cholesterol into functional docking and fusion platforms. Our results suggest that cholesterol opens pores directly by reducing the fusion-pore bending energy, and indirectly by concentrating several SNAREs into individual fusion events.

INTRODUCTION

A critical step in processes such as neurotransmitter or hormone release via exocytosis, intracellular trafficking, and enveloped virus infection is the creation of a fusion pore that connects membrane-enclosed compartments and allows the contents to be released (1). Most intracellular membrane fusion events, as well as exocytosis, are driven by soluble *N*-ethylmaleimide-sensitive factor attachment protein receptor (SNARE) proteins when vesicle-associated SNAREs (v-SNAREs) form complexes with target-membrane-associated SNAREs (t-SNAREs) (2). Exocytotic fusion pores are highly dynamic and may flicker repeatedly between the open and closed states before either permanently closing or dilating (3–11) (Fig. 1).

The dynamics of the pore are physiologically regulated and determine the amount, the size, and the kinetics of cargo release, with important consequences for downstream events. In chromaffin cells, basal stimulation selectively releases only small cargo through flickering fusion pores, whereas increased stimulation leads to release of all cargo sizes through pores that rapidly dilate (12). Although more challenging to detect, pore flickering also occurs during synaptic vesicle exocytosis (4,13,14) and may serve to regulate synaptic strength (15) and/or the kinetics and spatial extent of receptor activation (4).

Fusion-pore dynamics are altered by mutations in SNAREs and other components of the fusion machinery (5,8,16). Cholesterol, a major constituent of eukaryotic plasma membranes (40% (17)), synaptic vesicles (~40% (18)), and secretory granules (25% (19)), is also a key modulator of fusion-pore dynamics and rates of fusion. Pharmacological reduction of cholesterol lowered rates of exocytosis in hippocampal neurons (20) but shortened the duration of the prespike foot (PSF) in chromaffin cells, suggesting a faster transition to a fully developed pore (21). The

Submitted December 12, 2014, and accepted for publication February 4, 2016.

*Correspondence: erdem.karatekin@yale.edu or bo8@columbia.edu

Jason M. Warner, Zhenyong Wu, and Joerg Nikolaus contributed equally to this work.

Editor: Axel Brunger.

http://dx.doi.org/10.1016/j.bpj.2016.02.019

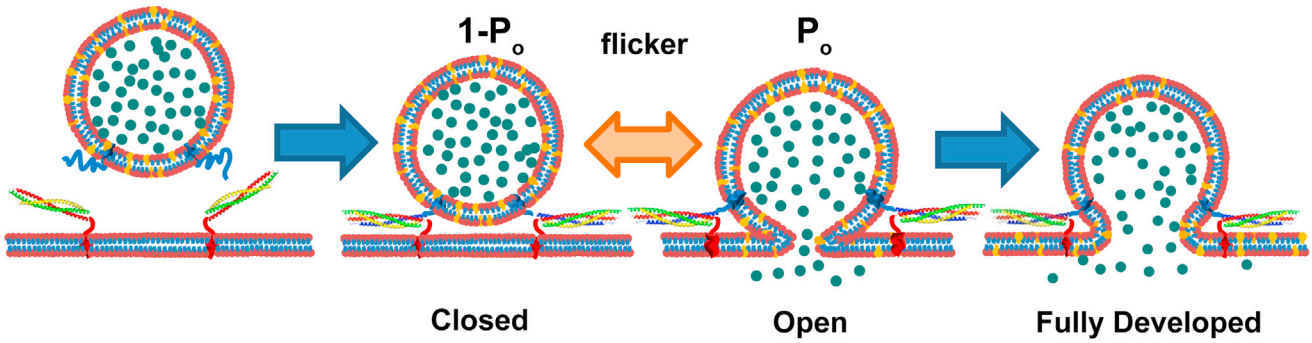

FIGURE 1 Schematic of the flickering dynamics of membrane fusion pores. A vesicle docks onto a planar membrane by complexation of vesicle v-SNAREs (*blue* on vesicle) with t-SNAREs (*red*, *yellow*, and *green* on SBL). Fusion of the membranes creates an open pore through which contents are released. Live-cell electrophysiological studies show that fusion pores may flicker rapidly and repeatedly between closed and open states, then dilate to become fully developed pores or permanently close. In this study, we track flickering of fusion pores by monitoring release of labeled vesicle membrane lipids (*yellow*) into the planar membrane (Fig. 2). Simultaneous observations of lipid and content release are also made (Fig. 3). Release is retarded because the pore is open only a fraction, P_o, of the time. To see this figure in color, go online.

presence of oleic acid, with an inverted cone geometry similar to that of cholesterol, reduced the PSF duration in PC12 and chromaffin cells (22). Introduction of ~40% cholesterol to liposome membranes increased the initial rates of fusion in a bulk liposome assay (23). In cell-cell fusion mediated by the influenza fusion protein hemagglutinin, cholesterol accelerated and increased the incidence of fusion (24).

Flickering dynamics of fusion pores are most directly measured using electrophysiological and electrochemical approaches. In amperometric traces of content release, pore flickering causes fluctuations in the low-amplitude PSF and in "stand-alone feet" that signal transient events involving partial content release without full pore enlargement (3–7). Flickering is also manifested by fluctuations in pore conductance (7,9) and membrane capacitance (11,14). From such studies, fusion pores that flicker typically do so ~2–10 times at frequencies from 40 Hz in beige mast cells to 170 Hz in chromaffin cells to 4000 Hz in ventral midbrain neurons (3,4,7). A pore height of ~15 nm, similar to that of a gap junction, is commonly assumed, in which case measured conductances imply pore radii of ~0.5–5 nm (9,11,13,14).

In small vesicles, pores were measured to flicker between two discrete states, the closed state and an open state of fixed size that varies little within or between flickering episodes. In ~25-nm-radius synaptic vesicles and microvesicles, conductance of fusion pores revealed ~10- to 20-Hz flickering between discrete open and closed states, with sharp transitions between the two and an almost constant conductance in the open state from one open event to another (13,14). In amperometric measurements of fusion pores in ~25 nm synaptic vesicles during exocytosis in ventral midbrain neurons, the initial peak value in flickering sequences was consistent between events, suggesting a fixed fully open pore state (4). In larger, ~100 nm dense-core vesicles in chromaffin cells, before dilation, flickering pores in the fully open state had approximately constant conductance from flicker to flicker, whereas pores in $\gtrsim$ 1-μm-sized large granules in beige mast cells show much more variable conductance in time during flickering (7,25,26).

A quantitative characteristic of a two-state flickering pore is its openness, P_o, the fraction of time the pore is in the open state. The analogous concept is used in the study of ion channels (27). The openness is closely related to the thermodynamic driving force for fusion, ΔF_{pore}, the free-energy difference between the open and closed states (Fig. 1). Using Boltzmann's distribution, $P_o = e^{-\Delta F_{pore}/k_BT}/(1+e^{-\Delta F_{pore}/k_BT})$, where T is temperature and k_B is Boltzmann's constant. ΔF_{pore} presumably sums downhill contributions from SNAREs and other components that drive the pore to open and uphill contributions from the lipid membranes that must bend to make the fusion pore (28). In a natural generalization to a flickering pore whose size fluctuates through a continuum of sizes, P_o is the time-averaged conductance relative to the conductance when fully open. Electrophysiological measurements suggest that P_o ~ 0.3–0.8, i.e., small free-energy differences, ΔF_{pore}, of order kT (3,4,7,10,13,14).

The mechanism that governs pore flickering is unknown, in part because methods to measure individual pore dynamics in reconstituted, biochemically defined systems have not been available. Here, we developed such a method, using total internal reflection fluorescence (TIRF) microscopy to measure flickering pores during reconstituted SNARE-mediated fusion of small unilamellar vesicles (SUVs; comparable in size to synaptic vesicles) with supported bilayers (SBLs). Due to the evanescent wave excitation with a polarized laser beam (29), individual fusion events are signaled by a rapid increase in intensity as fluorescently labeled lipids diffuse from the vesicle membrane into the SBL membrane. Consistent with rapid ($\gtrsim$ 100 Hz) pore flickering, lipids were released from the vesicle ~10-fold, and in some cases up to 100-fold, more

slowly compared to release via a continuously open pore (Fig. S1 in the Supporting Material). In experiments where we simultaneously monitored both lipid and soluble cargo release through the fusion pore, content release occurred with similar or slower kinetics compared to lipid release, also consistent with a rapidly flickering pore. Most fusion pores reseal after releasing only part of their contents. Events compatible with hemifusion (where proximal leaflets fuse, but not distal leaflets) were extremely rare. Overall, the retardation of lipid release we observe is very likely due to pore-flickering dynamics, rather than to diffusional barriers due to high curvature effects or the presence of proteins that may line the fusion pore.

From the lipid release time, we calculated the pore openness, P_o (Fig. 1), and vesicle size for each event. For most lipid compositions, lipid bilayers controlled pore flickering: SNAREs had little effect, and cholesterol increased pore openness, consistent with its ability to lower fusion-pore membrane bending energy. With higher, physiological cholesterol levels in target membranes, the presence of SNAREs dramatically opened flickering pores. Thus, in addition to its direct role, cholesterol synergistically facilitates pore opening by SNARE proteins. Our results suggest that this effect derives from cholesterol-mediated clustering of t-SNAREs at the fusion site.

MATERIALS AND METHODS

Materials

1-palmitoyl-2-oleoyl-*sn*-glycero-3-phosphocholine (POPC), 1,2-dioleoyl-*sn*-glycero-3-phosphocholine (DOPC), 1-stearoyl-2-arachidonoyl-*sn*-glycero-3-phosphoethanolamine (SAPE), 1,2-dioleoyl-*sn*-glycero-3-phospho-(1′-myo-inositol-4′,5′-bisphosphate) (PI(4,5)P2), 1,2-dioleoyl-*sn*-glycero-3-phosphoethanolamine-N-(lissamine rhodamine B sulfonyl) (LR-PE), 1,2-dioleoyl-*sn*-glycero-3-phosphoethanolamine-N-(7-nitro-2-1,3-benzoxadiazol-4-yl) (NBD-PE), 1,2-dioleoyl-*sn*-glycero-3-phosphoethanolamine-N-[methoxy(polyethylene glycol)-2000], and cholesterol were purchased from Avanti Polar Lipids (Alabasater, AL). PI(4,5)P2, only found in plasma membranes (30), and NBD-PE, used to check SBL fluidity using fluorescence recovery after photobleaching (31), were included only in the t-SNARE SBLs. In some experiments, instead of LR-PE, we used the lipid probes 1,1′-dioctadecyl-3,3,3′,3′-tetramethylindocarbocyanine perchlorate (DiI, or DiIC18 (3); D-282, Invitrogen, Carlsbad, CA) or 1,1′-dioctadecyl-3,3,3′,3′-tetramethylindodicarbocyanine perchlorate (DiD, or DiIC18 (5); D-307, Invitrogen). The soluble content marker sulforhodamine B (SRB; S-1307, Invitrogen) was purchased from Invitrogen.

Recombinant protein expression and purification

Recombinant VAMP2, syntaxin-1, and SNAP25 were expressed, purified, and reconstituted into SUVs, as described in detail previously (31,32). We used lipid/protein ratios of 200 and 20,000 for the v-SUVs and t-SBLs, respectively. Even for the smallest v-SUVs (R_{ves} = 10–20 nm), this provides enough copy numbers (5–17) of externally facing v-SNAREs per SUV, because efficient fusion in this assay requires $\gtrsim$5 SNARE complexes (32). Thus, our results for the number of t-SNAREs recruited for fusion (see Fig. 5 *A*) are not limited by the number of v-SNAREs present on vesicles.

Preparation of SUVs and SBLs

For experiments monitoring lipid mixing alone, we used the method of (31,32), but with different lipid compositions, as in Table 1 (SUV and SBL compositions are listed separately in Tables S1 and S2). We included either 0.8 mol % LR-PE or 1 mol % DiI as lipid markers, except in the case of α^{+}_{chol}, where 0.62 mol % LR-PE was used (Table S1).

For simultaneous monitoring of both lipid and content release, we included 1 mol % DiD as the lipid marker and encapsulated the soluble content marker SRB into v-SUVs. To do so, we followed the protocol of Kyoung et al. (33), with the following modifications. Dilution of the lipid, protein, and detergent mixture was followed by dialysis against 4 L of buffer overnight at room temperature. v-SUVs were then passed through a CL-4B column (Sepharose CL-4B, 17-0150-01, GE Healthcare, Little Chalfont, United Kingdom) to remove free SRB. SRB concentration was 10 or 50 mM. The lipid/protein ratio for v-SUVs was 200, as in single-color lipid-mixing experiments. We used the following lipid compositions for the v-SUVs: 67:12:15:5:1 POPC/DOPS/SAPE/PEG2KPE/DiD or 23.55:12:15:45:3.45:1 POPC/DOPS/SAPE/Ch/PEG2KPE/DiD. The t-SBLs contained one t-SNARE complex for every 20,000 lipids and were composed of 64.5:12:15:3:5:0.5 POPC/DOPS/SAPE/PIP2/PEG2KPE/NBD-PE.

Microfluidic flow channels and microscopy

Fabrication of microfluidic flow channels, formation and characterization of t-SNARE-reconstituted SBLs in the channels, and detection of fusion events are described in detail in Karatekin and Rothman (31). In this assay, fusion of single v-SNARE reconstituted liposomes (v-SUVs) with t-SNARE-bearing SBLs is observed at frame rates of 32/s (full frame) to 60/s (from a cropped region of interest). These correspond to frame durations of 31 and 17 ms, respectively. Frame durations <~15 ms resulted in lower signal/noise ratios that made tracking of single LR-PE fluorescently labeled lipids difficult. One pixel corresponded to 267 nm in the sample plane. LR-PE or DiI fluorescence was excited using an s-polarized (perpendicular to the plane of incidence) 532 nm laser beam.

To determine the areal lipid density in the membranes, $\rho_{lip} = 1/(f_{lip}\, a_{lip})$, where f_{lip} is the fraction of lipids that are labeled, we assumed a lipid headgroup area of $a_{lip} = 0.8$ nm^2 for PC/PS/PE/PIP2 and PC/PS compositions and $a_{lip} = 0.6$ nm^2 for PC/PS/PE/PIP2/Ch+ and PC/PS/PE/PIP2/Ch compositions (34).

Some of the data were obtained using an inverted microscope (IX81, Olympus, Center Valley, PA) equipped with an EM-CCD camera (iXon Ultra, Andor, Belfast, United Kingdom) and the Olympus CellTIRF TIRF microscopy (TIRFM) accessory. The microscope and data acquisition were controlled by Micro-Manager (University of California San Francisco). A 100×/1.49 NA oil TIRF objective (UAPO N, Olympus) was used. All experiments were carried at 32°C (Thermo Plate TOKAI HIT, Olympus). Images were collected with a frame duration of 17 ms (full frame). We used a 488 nm laser for FRAP measurements and a 561 nm laser for detecting LR-PE or DiI during fusion.

TABLE 1 Lipid Compositions Used in This Study

	Ch (%)	PC (%)	PS (%)	PE (%)	PIP2 (%)
POPC/DOPS/SAPE/PIP2	–	60/64	14/14	18/18	4/0
POPC/DOPS/SAPE/PIP2/Ch	10/45	55/24	12/12	15/15	3/0
POPC/DOPS/SAPE/PIP2/Ch+	45/45	19/23	12/12	15/15	3.9/0
DOPC/DOPS	–	80/79	15/15	–	–

Each entry shows the two mole fractions in the SBL membrane/vesicle membrane. In addition, each composition contained 3.45–5.0 mol % PEG2KPE, and 0.6–1.0 mol % lipid marker (LR-PE, DiI, or DiD, the latter only for content-release experiments). See Materials and Methods and Tables S1 and S2 for details.

To estimate the evanescent field penetration depth, we measured the angle of incidence, θ, of the excitation beam with respect to the normal to the imaging plane, and used the expression $\delta_{TIRF} = \lambda_o/4\pi\,(n_g^2 \sin^2\theta - n_w^2)^{-1/2}$ (29), where $\lambda_o = 532$ nm is the laser wavelength, and $n_g = 1.52$ and $n_w = 1.33$ are the refractive indices of glass and water, respectively. For this, we coupled a 2 cm × 2 cm × 2 cm BK7 glass cube (Thorlabs, Newton, NJ) to the TIRF objective using oil that matched the refractive index of glass. At angle θ, used to generate TIR in the fusion experiments, the beam went undeflected into the cube and emerged from one side refracted at the glass-air interface and projected onto a wall. Simple geometry based on the beam position on the wall and the position of the objective, along with the known refraction at the cube-air interface, allowed calculation of the incidence angle, $\theta = 73.5$–$77.4°$ ($\delta_{TIRF} = 65$–71 nm), with the highest intensity spot at 75°, corresponding to $\delta_{TIRF} = 68$ nm. This value is used in the subsection The size of a docked vesicle can be directly inferred from the docked vesicle intensity in TIRFM (and see Fig. 6 *D*).

Single lipid-label measurements

We tracked single lipids using ImageJ and Speckle TrackerJ, the tracking plugin described in (35). For details, see Fig. S2, *A–C*.

Analysis of single-vesicle events

We identified fusing vesicles by eye and tracked them using the ImageJ plugin Speckle TrackerJ (35). We used fusing vesicle trajectories to train Speckle TrackerJ to track the remaining vesicles that dock. For each fusion event, the total intensity in a region of interest was computed with Matlab from the trajectories obtained from SpeckleTrackerJ.

Curve fitting

We performed all curve fitting using the Curve Fitting Toolbox in Matlab with linear or nonlinear least-squares optimization.

Simultaneous detection of lipid and content release

For these experiments, we used an Olympus IX81 microscope, custom-modified for polarized TIRF excitation and two-color detection. SRB and DiD fluorescence was excited using 561 nm (04-01 series, Cobolt Jive, Solna, Sweden) or 638 nm (LuxX, Omicron Laserage, Rodgau-Dudenhofen, Germany) lasers, respectively, through an Olympus PlanApo 60×/1.45 Oil TIRF objective, using *s*-polarized light. We split the emission using a 640 nm dichroic mirror (ZT640rdc-UF2, Chroma, Bellows Falls, VT), and projected the two beams that went through a short (570–620 nm; ET595/50m EM, Chroma) and a long (662.5–737.5 nm; ET700/75m EM, Chroma) wavelength emission filter side-by-side on the same electron-multiplying charge-coupled device (Ixon Ultra, Andor). One pixel corresponded to 265 nm. Exposure time was 17.8 ms (duty cycle, 18.3 ms). We recorded 3,300 frames (60 s) for a total of 26 movies. Image stacks were analyzed using ImageJ and home-made Python scripts.

RESULTS

Single-event TIRF-based fusion assay

We used a recently established TIRFM-based fusion assay (31,35) to monitor fusion of individual, neuronal v-SNARE-containing SUVs with neuronal t-SNARE-reconstituted planar bilayers supported on a soft poly(ethylene glycol) (PEG) cushion in microfluidic flow channels, with 0.8 mol % LR-PE or 1 mol % DiI as fluorescent lipid markers (Fig. 2 *A*).

Four membrane lipid compositions were tested (Table 1): a model DOPC/DOPS mixture (31,32,36) and three compositions that included PI(4,5)P2 in SBL membranes and SAPE and varying amounts of cholesterol, 0%, 10%/45%, and 45%/45%, in the SBL/SUV membranes (POPC/DOPS/SAPE/PIP2, DOPC/DOPS/SAPE/PIP2/Ch, POPC/DOPS/SAPE/PIP2/Ch+, see Table 1 and Materials and Methods). All lipid compositions used in this study are expected to form fluid bilayers, as the transition temperature of each component is <0°C. Accordingly, we saw no evidence of phase separation, either using fluorescent probes or when we tracked single lipid labels. PE is found at levels up to 15% in synaptic vesicles, secretory granules, and plasma membranes (18), has negative spontaneous curvature, and promotes fusion in model systems (37). The signaling lipid PI(4,5)P2 is present in small amounts in the inner leaflet of

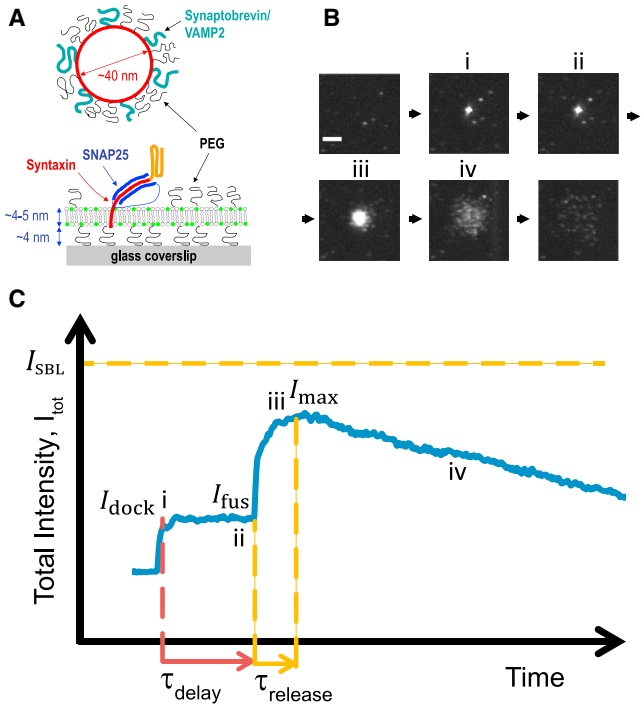

FIGURE 2 Using TIRFM to measure lipid mixing and fusion-pore flickering dynamics. (*A*) Vesicles reconstituted with v-SNAREs (synaptobrevin/VAMP2) fuse with a target SBL reconstituted with cognate t-SNAREs (syntaxin and SNAP25). Membranes are PEGylated to prevent nonspecific interactions, and 0.6–1% of lipids are fluorescently labeled. (*B*) TIRF sequence during a typical fusion event, viewed from beneath the coverslip in (*A*). When the vesicle docks onto the SBL, a spot appears (*i*). At a later time, τ_{delay}, fusion occurs (*ii*) and the spot brightens as labeled lipids diffuse into the SBL (*ii*→*iii*). Individual lipids are discernible by stage iv. The box size is 22 μm × 22 μm, 82 × 82 pixels, and the scale bar represents 5 μm. (*C*) Typical time course of total fluorescence intensity, I_{tot}, integrated over the box in (*B*), from which we extracted the lipid release time, $\tau_{release}$. After lipid release into the SBL, I_{tot} would increase to the value I_{SBL} were it not for bleaching (*iii*→*iv*) ($I_{max} < I_{SBL}$). To see this figure in color, go online.

the plasma membrane (1–2%) (30) and interactions with the t-SNARE syntaxin concentrate PIP2 at docking and fusion sites (38). Cholesterol plays a facilitating role in biological and model fusion reactions that is well-documented (20,23,24), including its modulation of the fusion pore (21).

Lipid compositions used in this study

For most experiments, we recorded movies of docking and fusion events, monitoring only lipid markers. For each fusion event, we measured the total intensity versus time, $I_{tot}(t)$, summed over all pixels in a box drawn around the fusing vesicle (Fig. 2, *B* and *C*). After docking of a vesicle to the SBL, when the intensity increases to a value I_{dock}, after a delay time, τ_{delay}, fusion is announced by a rapidly increasing intensity (39) as labeled lipids, initially in the vesicle membrane, begin to be released into the SBL through the bilayer walls of the fusion pore (Fig. 1). The intensity of labeled lipids in the vesicle, LR-PE or DiI, is reduced by a certain average factor, λ_{TIRF}, because the evanescent excitation field, with a decay length of ~68 nm (Materials and Methods), decays with distance from the SBL, and its polarization is a worse match for the dipole orientations of the fluorescent lipid labels when they reside in the spherical vesicle (29). The delay time distributions revealed a fast-fusing SNARE-mediated population and a slowly fusing, nonspecific population (32) (Fig. S2, *E* and *F* and Supporting Material).

Lipid and content release are retarded by flickering fusion pores

We used the fluorescence increase that accompanies diffusion of a labeled vesicle lipid into the SBL to track the release process and hence infer properties of the fusion pore. The fluorescence increases by the inverse of the mean intensity reduction factor for lipids in the vesicle, λ_{TIRF}. As the increase is instantaneous upon lipid transfer, we could measure the fraction of lipids transferred with high sensitivity and with temporal resolution limited only by acquisition frame rates (up to ~100 Hz), not by the time required for the lipids to diffuse a distance larger than the optical resolution (~250 nm) to detect their spread. Individual lipid labels became discernible as they diffused away from the fusion site, eventually disappearing in single bleaching steps (35). The release of lipids into the SBL occurred over a timescale, $\tau_{release}$, when the intensity increased toward a plateau but then decreased due to bleaching (Fig. 2 *C*).

Intriguingly, lipid release times were far greater (~30–250 ms; Fig. S1) than expected for a permanently open pore (~10 ms, the lipid diffusion time on the scale of a typical vesicle (40)). This suggested that fusion pores were flickering and spending only a fraction of the time in the open state, i.e., the pore openness, P_0, was significantly less than unity.

To test this possibility, we studied fusion events while simultaneously monitoring lipid and content release. We encapsulated 10 or 50 mM soluble content label SRB into v-SUVs that also contained 1 mol % DiD as the lipid marker. We excited both markers simultaneously using 561 nm (for SRB) and 638 nm (for DiD) lasers. We split the emission into two beams that went through short (570–620 nm) and long (662.5–737.5 nm) wavelength filters for the SRB and DiD emissions, respectively, and projected the two emission signals side by side onto an EMCCD chip. Movies were recorded with 18.3 ms time resolution for 60 s. SRB was encapsulated into vesicles at highly self-quenched concentrations. Consequently, for most docked vesicles, initially only the DiD lipid signal was visible. However, within a frame after the lipid signal began to increase due to transfer of lipids into the SBL, the content signal also began to increase due to dequenching effects caused by dilution of the content labels as molecules escaped through the fusion pore (Fig. 3). For >80% of all events for which simultaneous lipid and content release could be observed (74 of 91 events), the initial pore resealed after releasing all of the lipid labels but only a fraction of the content labels. More than 20% of these partial-content-release events were followed seconds later by a sudden decrease in content signals (Fig. S7). We presumed this was either because the pore reopened with sufficient width to allow rapid release of contents, or because the vesicle burst due to accumulated photodamage (41). Whatever its origin, the late disappearance of content signal showed that the initial increase in content signal was not due to content markers being released and then trapped in the space between the SBL and the substrate, as found in a previous study using SBLs directly supported on a quartz substrate, without a soft spacer such as the PEG layer used here (41).

Content- and lipid-release kinetics either occurred at comparable rates within a few frames (24/91 events), or content release was visibly slower (46/91 events; see Fig. 3 for an example). For the remaining events, we could not reliably compare the kinetics.

Signal changes compatible with hemifusion (lipid mixing preceding content mixing) were observed very rarely (2 of 91 events). Hemifusion could also be detected in single-color experiments monitoring lipid labels alone, as it would leave about half the initial docked-vesicle lipid intensity intact after dispersion of the outer-leaflet lipid markers into the SBL (31,32). Monitoring lipid signals alone, we found that such events were very rare, consistent with our previous studies (31,32).

In summary, simultaneous monitoring of lipid and content release showed that the two processes commenced within a single frame of one another (18.3 ms), and the kinetics of both content and lipid release were much slower than expected for permanently open pores $\gtrsim$ 2 nm in

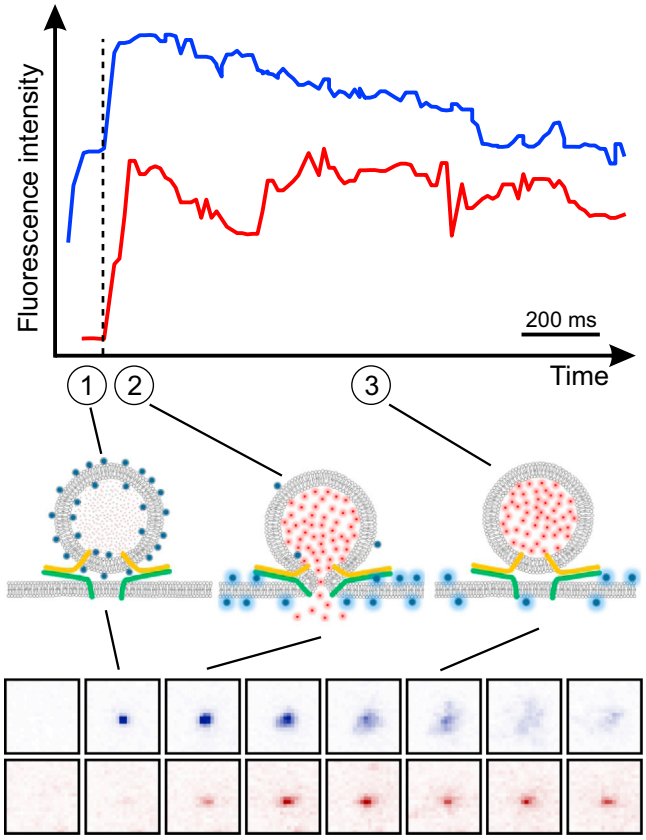

FIGURE 3 Simultaneous content and lipid release using TIRFM. v-SUVs contained 1 mol % DiD lipid dye and encapsulated 10 or 50 mM soluble content marker SRB. DiD and SRB were excited simultaneously using 638 nm and 561 nm laser lines, respectively. The emission was split and filtered to observe DiD (*top*, *blue trace*) and SRB (*lower*, *red trace*) fluorescence signals simultaneously projected onto an EMCCD detector. Total intensities from a region 20 pixels × 20 pixels (5.3 μm × 5.3 μm) is plotted for both the lipid (*upper*, *blue trace*) and content (*lower*, *red trace*) signals for a representative event. Snapshots from the lipid (*top sequence*, *blue*) and content (*bottom sequence*, *red*) signals are shown in inverted false color. When docking was clearly visible in the lipid channel, the content channel was still dim, because SRB was encapsulated at self-quenching concentrations (*1*). In the same frame where the lipid signals start to increase, announcing lipid mixing, the content signals also increase (*dashed vertical line*) due to dilution and dequenching of encapsulated SRB as some molecules escape through the pore. Once lipid transfer is complete (shortly after the maximum in the *upper blue trace*), the intensity in the lipid channel decreases due to photobleaching, as in Fig. 2. The SRB signals remain stable after lipid release (but bleach slowly (*3*)), indicating that the pore resealed after partial release of contents. In this example, initial lipid and content release occurred with comparable kinetics (*2*) within a few frames (each 18.3 ms apart). In other cases, release was markedly slower (see Fig. S7). To see this figure in color, go online.

diameter. These findings strongly suggest that the fusion pores we observe flicker, and the effect is to retard both lipid and content mixing. We note that during fusion reactions mediated by the influenza fusion protein hemagglutinin, electrophysiologically detected fusion pore opening preceded detectable lipid and content release by seconds (42). Zimmerberg et al. (42) argued that this was caused by an early transition to a larger pore rather than by retardation due to the effect of fusion proteins, as previously proposed (43). Our results suggest that the size and flickering dynamics of the pore itself set lipid and content release rates, since the onset of both was simultaneous. Moreover, retardation of lipid diffusion was the same for specific and nonspecific fusion, suggesting that the retardation is not caused by the SNARE proteins (Fig. 4 *C*).

For the remainder of the study, we used lipid release kinetics to characterize the flickering statistics of fusion pores, as the signal/noise ratio in single-color measurements of lipid release allowed tracking of single lipid labels and calculation of vesicle size for individual events. This was needed to compute the pore openness, as detailed below. Unless specified otherwise, all experimental results presented below are from single-color lipid-marker measurements.

Fusion pore openness, P_0, is quantitatively related to the lipid release time, $\tau_{release}$

We established a relationship that enabled us to deduce the pore openness, P_o, from the time for lipids to be released from the vesicle into the SBL, $\tau_{release}$, that we measured for each fusion event from the TIRFM intensity curve (Fig. 2 *C*). A mathematical model of lipid release through a flickering pore showed that

$$P_o = \frac{A_{ves} b}{2\pi r_p D_{lip} \tau_{release}} \quad (1)$$

(see Supporting Material). For a two-state (open/closed) pore, P_o is the fraction of the time in the open state, but Eq. 1 is equally valid for a flickering pore with a size varying continuously in time, when P_o is the time-averaged pore radius relative to the fully open radius. In Eq. 1, A_{ves} is the vesicle area and D_{lip} the lipid diffusivity, which we measured directly (see below). This equation states that $P_o = g\,\tau_{ves}/\tau_{release}$, where $\tau_{ves} = A_{ves}/D_{lip}$, the time for a lipid to diffuse a distance of the order of the vesicle size, would be the diffusion-controlled release time for a fully open pore (to within logarithmic corrections). For an infrequently open pore, $P_o < 1$, the release time, $\tau_{release}$, is much greater than τ_{ves}. P_o is the ratio of these two timescales times a factor $g = b/2\pi r_p$ reflecting the role of pore geometry on lipid release rate.

We took a pore height of $b = 15$ nm, as is commonly assumed, and the radius of the fully open conducting pore was taken to be 1 nm, as reported for smaller vesicles (4,9,11,13,14). This implies a value of $r_p = 3$ nm as the fully open pore radius in Eq. 1 is the effective value seen by a diffusing lipid and so includes half the bilayer thickness, taken to be 2 nm (Fig. S1 *A*). Equation 1 states that a flickering pore more often in the closed state (lower P_o) releases lipids more slowly (larger $\tau_{release}$).

For a given fusion event, the vesicle area, A_{ves}, in Eq. 1 is unknown, as sizes varied significantly. The docked

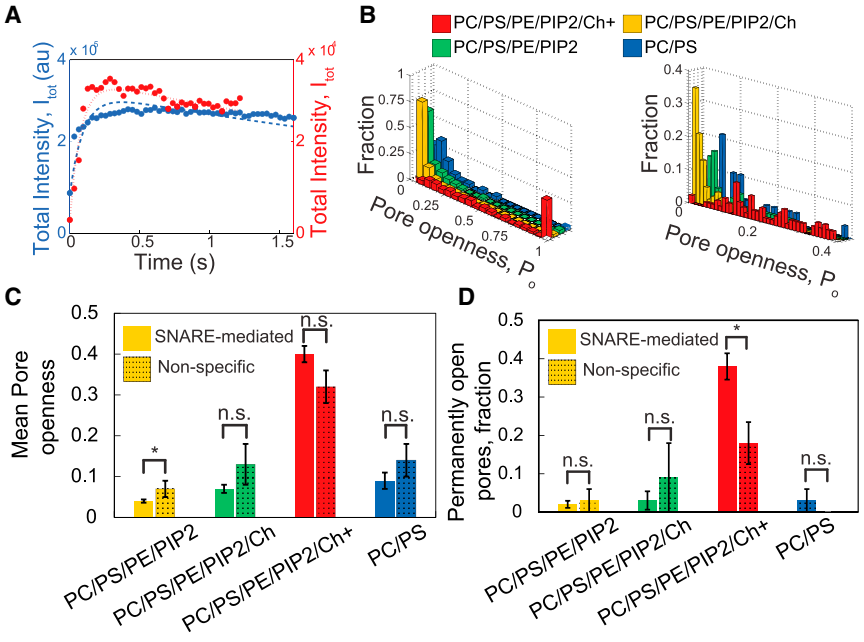

FIGURE 4 Openness statistics of SNARE-mediated flickering fusion pores. (*A*) TIRF intensity versus time after fusion for two typical SNARE-mediated fusion events. The time course of the red trace (*short-dashed curve fit*, PC/PS) is well fit by Eq. 3 for a flickering pore, with openness $P_o = 0.09$ (*short-dashed curve*). The fit from Eq. 3 is poor for the blue trace (*long-dashed curve fit*, PC/PS/PE/PIP2/Ch+, 45% cholesterol), with nominal $P_o = 3.48$ (*long-dashed curve*), flagging a permanently open pore (Eq. 4). (*B*) SNARE-mediated fusion pores flicker and are dramatically opened by increasing cholesterol content. (*Left*) Flickering-pore openness, P_o, and the fraction of pores that are permanently open ($P_o = 1$ column) for each of the four lipid compositions studied (Table 1). The bin size is 0.05. (*Right*) Blowup of $P_o \leq 0.4$ data (bin size, 0.01). (*C* and *D*) SNAREs play little or no role in fusion-pore flickering unless cholesterol content is high. Mean pore openness (*C*) and fraction of pores that are permanently open (*D*) versus composition for SNARE-mediated and SNARE-independent fusion-pore dynamics. Error bars in (*C*) and (*D*) indicate the mean ± SE; $^*p < 0.05$ using Student's *t*-test. To see this figure in color, go online.

vesicle intensity, I_{dock} (Fig. 2 *C*) is the best measure of vesicle size, being the earliest and least affected by bleaching. The difficulty is that the relation between A_{ves} and I_{dock} is not a priori known, since the intensity of fluorescently labeled lipids in the vesicle is unknown. However, we directly measured I_{lip}, the single lipid intensity for lipids in the planar SBL (see below). Thus, we used the TIRFM curve for each event to determine the fluorescence intensity reduction factor, λ_{TIRF}, namely the ratio of total intensities before and after lipid release. The area is then

$$A_{ves} = I_{dock} / \left(\lambda_{TIRF} I_{lip} 2\rho_{lip}\right). \quad (2)$$

Here, ρ_{lip} is the areal density of fluorophores in each leaflet of the vesicle membrane and $\lambda_{TIRF}\, I_{lip}$ is the single labeled lipid intensity for a lipid in the vesicle, averaged over all locations in the vesicle membranes, including the reduction factor, λ_{TIRF}, relative to the value I_{lip} in the SBL. The reduction factor depends on vesicle size in a complex fashion (see below).

In practice, direct extraction of $\tau_{release}$ and λ_{TIRF} from the measured fluorescence signal, $I_{tot}(t)$, is difficult due to bleaching of labeled lipids in the SBL, with bleaching time, τ_{bleach}, of ~3.5 s for LR-PE (Figs. 2 *C* and S2 *C*). Thus, we used the expression predicted by our model for the TIRFM signal, given by

$$\frac{I_{tot}(t)}{I_{fus}} = e^{-t/\tau_{release}} + \frac{\left(e^{-t/\tau_{bleach}} - e^{-t/\tau_{release}}\right)}{\lambda_{TIRF}\left(1 - \tau_{release}/\tau_{bleach}\right)} \quad (3)$$

(see the Supporting Material). We neglect the slower bleaching in the vesicle (τ_{bleach} ~ 18 s; Fig. S2 *D*). Our procedure was to fit the predicted expression (Eq. 3) to the experimentally measured signal and determine the two crucial parameters $\tau_{release}$ and λ_{TIRF} as best-fit parameters. A related situation was mathematically modeled in (44), in which labeled lipids diffused through a narrow pore during cell-cell fusion and the effects of fluorescence dequenching were calculated.

Permanently open pore

In the above, lipid release is limited by flickering, and the fraction of labeled lipids remaining in the vesicle a time *t* after the instant of fusion (when the pore first opens) decays exponentially, $\phi_{ves} = e^{-t/\tau_{release}}$ (Eq. S8). We will see that our experiments show that a fraction of pores do not flicker, but are permanently open. In this case, release is limited by diffusion, and our model shows that the decay has a qualitatively different inverse time dependence and the TIRFM intensity time course is different:

$$\frac{I_{tot}(t)}{I_{fus}} = e^{-t/\tau_{bleach}}\left[\phi_{ves}(t) + \left(\frac{1 - \phi_{ves}(t)}{\lambda_{TIRF}}\right)\right], \quad (4)$$
$$\phi_{ves}(t) = \tau_{ves}/t.$$

SNARE-mediated fusion pores flicker or are permanently open

We used the following procedure, which yielded the pore openness, the vesicle radius, R_{ves}, and the intensity reduction factor, λ_{TIRF}, for each fusion event. 1) We first measured the bleaching time, τ_{bleach}, the diffusivity, D_{lip}, and the intensity, I_{lip}, of single fluorescently labeled lipids in the SBL (Materials and Methods and Fig. S2). 2) For each detected

fusion event, we extracted the docked fusion intensity, I_{dock}, and the intensity at the instant of fusion, I_{fus}, from the measured fluorescence intensity curve, $I_{tot}(t)$ (Fig. 2 *C*). 3) We fit the predicted TIRF intensity curve, $I_{tot}(t)$ (Eq. 3), to the experimental curve using the fluorescence reduction factor, λ_{TIRF}, and lipid release time, $\tau_{release}$, as fitting parameters. 4) We used Eq. 2 to obtain the vesicle area and radius, and then Eq. 1 to obtain the pore openness.

Applying this procedure to the fast SNARE-mediated fusion events we found that pores flickered with pore openness of $0.01 \lesssim P_o \lesssim 0.9$, suggesting free energies of pore formation of $-2\ \mathrm{kT} \lesssim \Delta F_{pore} \lesssim 5\ \mathrm{kT}$ (Fig. S1 *B*). Although most pores flickered, in many cases, the analysis returned a nominal P_o value exceeding unity, indicating a fully open pore, $P_o = 1$. To reinforce this conclusion, we tested these pores for inverse time-release kinetics, $\phi_{ves} \sim 1/t$, the signature of a permanently open pore (Eq. 4). For this test, we used larger vesicles, $R_{ves} \geq 25$ nm, whose slower release kinetics were more accessible. The exponent of the best-fit power law to the pooled release kinetics was close to that predicted (-0.99 ± 0.22), compared to a best-fit exponent of -0.68 ± 0.09 for flickering pores with $P_o < 0.15$ (Fig. S3 *B*).

As an additional test of our assumption that slow lipid release reflects flickering pores (Eq. 3) rather than restricted lipid diffusion due to high curvature or protein crowding effects at the pore (45) we repeated experiments using a different label, replacing LR-PE with DiI. We found statistically insignificant differences in pore openness values (Supporting Material and Fig. S6), consistent with normal lipid diffusion through the pore.

We note that a "permanently" open pore is one that remained open long enough to release all labeled lipids, approximately the lipid diffusion time for the vesicle size, τ_{ves} (multiplied by a logarithmic factor of order unity involving the pore diameter (40)). Thus, such a pore could in fact be slowly flickering, with a frequency of $\lesssim 100$ Hz if we take a typical τ_{ves} ~10 ms. In fact, we found no vesicle size dependence in the fusion statistics (Supporting Material and Fig. S4), suggesting that such pores remained open for sufficiently long that even the largest vesicles studied (R_{ves} ~ 80 nm) had enough time to empty their labeled contents. For these large vesicles, this would occur in an estimated time of order τ_{ves} ~ 50 ms. This suggests that the pores we identify as open flickered at frequencies of <20 Hz.

Cholesterol promotes the open state of the fusion pore

When pore statistics were classified according to the composition of the fusing membranes, there was a strong correlation of flickering pore openness with the presence of cholesterol (Fig. 4, *B–D*). For cholesterol-free compositions, the mean flickering pore openness was $\overline{P_o} = 0.04$, although only ~2% were permanently open. With 45% (10%) cholesterol in the SUV (SBL) membranes, the mean P_o doubled, but the permanently open fraction was unchanged. For compositions better mimicking physiological conditions, which included 45 mol % cholesterol, the effect was dramatic: relative to cholesterol-free membranes, the flickering pore openness and the permanently open fraction increased ~10-fold and ~20-fold, respectively.

Our simultaneous lipid- and content-release measurements corroborated these findings. When v-SUVs and t-SBLs both lacked cholesterol, content labels were released more slowly than lipid markers in 54% of all events (43 of 79), both types of release occurred within a few frames for 22% of events (17 of 79), and the kinetics could not be reliably compared due to weak signals for 24% of events (19 of 79). In contrast, when the v-SUVs included 45 mol % cholesterol, both types of release occurred rapidly within a few frames in 58% of all events (7 of 12), whereas contents were released more slowly for only 25% of events (3 of 12). For 17% of events (2 of 12) we could not reliably compare release kinetics.

SNARE proteins have little effect on the fusion-pore openness unless physiological levels of cholesterol are present

To distinguish the respective roles of SNAREs and lipid bilayers in fusion-pore dynamics, we repeated the above analysis for the slow nonspecific fusion events, for which we assumed the fusion-pore dynamics are not SNARE mediated (32). Both without cholesterol and with 45% (10%) cholesterol in the SUV (SBL) membranes, these events showed pore openness and permanently open pore fractions that were statistically indistinguishable from SNARE-mediated events, except that there was a small increase in P_o with no cholesterol ($n = 353$ SNARE-mediated events, $m = 68$ nonspecific events, Fig. 4, *C* and *D*). This suggests that the lipid bilayers themselves governed pore dynamics with little influence from SNARE proteins.

To test this conclusion, we measured fusion between protein-free SBLs and v-SNARE-containing SUVs (Supporting Material and Fig. S2 *F*). For the same compositions, the delay times and openness were statistically indistinguishable from those for the slow component in the presence of v- and t-SNAREs. This is consistent with the hypothesis that pore dynamics for the slow component reflect the physical properties of lipid bilayers only.

A qualitatively different picture emerged at physiological cholesterol levels in all membranes (45%): SNARE proteins then increased the fraction of open pores significantly, from 18% to 38% (Fig. 4 *D*). Thus, at high concentrations cholesterol opens pores both indirectly, by activating SNARE-mediated pore opening, and directly through its influence on the lipid membranes.

With physiological amounts of cholesterol, fusion is so accelerated that there is insufficient time to recruit additional t-SNAREs to the fusion site after docking

Next, we examined the effect of cholesterol on the docking-to-fusion delay times for the fast SNARE-mediated fusion events, and we applied the model of (32), which assumes that fusion is limited by the diffusive recruitment of t-SNAREs to the fusion site once a vesicle has docked. Delays were ~2-fold greater in the presence of intermediate amounts of cholesterol (45% and 10% in the SUV and SBL membranes) and sufficient for three to six t-SNAREs to have been recruited, consistent with literature values for the number of SNAREs required for fusion (32,36) (see Fig. 5 *A* and Supporting Material).

By contrast, at physiological cholesterol levels (45% in all membranes), the delay times were ~3-fold smaller, too short for even one additional t-SNARE to have been diffusively recruited if one assumes a uniform spatial distribution of t-SNAREs. This was unexpected, since lipid diffusivity was reduced ~4-fold at these cholesterol levels (Table S3), suggesting that delay times would be greater. Thus, t-SNAREs were presumably already clustered at docking sites in sufficient numbers to trigger fusion, consistent with cholesterol-mediated t-SNARE clustering observed in cells (46–49).

Consistent with these results, the probability that a docked vesicle underwent SNARE-mediated fusion during the observation time increased ~3-fold at the highest cholesterol levels (Fig. 5 *B*).

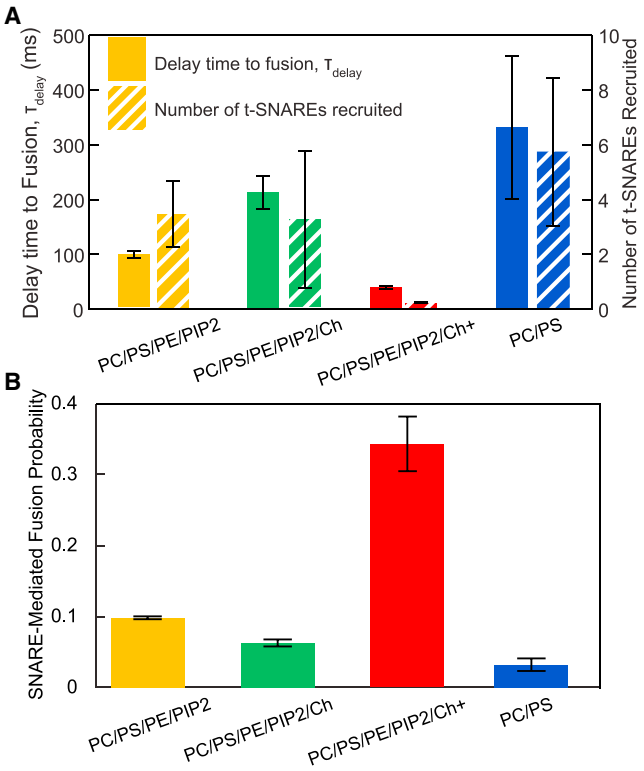

FIGURE 5 Physiological amounts of cholesterol accelerate fusion by clustering t-SNAREs. (*A*) Delay times to SNARE-mediated fusion after vesicle docking versus membrane lipid composition (*solid bars*) and calculated number of t-SNAREs assumed recruited by diffusion to the fusion site during the delay time (*striped bars*). Lower amounts of cholesterol (*yellow* (PC/PS/PE/PIP2) and *green* (PC/PS/PE/PIP2/Ch)) increase delay times, consistent with the reduced lipid diffusivities, but the number of t-SNAREs recruited for fusion is unchanged. At physiological cholesterol (PC/PS/PE/PIP2/Ch+), fusion is so accelerated that there is insufficient time to recruit any additional t-SNAREs after docking, suggesting that t-SNAREs are preclustered. (*B*) Physiological cholesterol levels increase the probability ~3-fold that a docked vesicle undergoes SNARE-mediated fusion (as opposed to nonspecific fusion or no fusion) before complete bleaching (~20 s). To see this figure in color, go online.

Fluorescence reduction factor and vesicle size are unique functions of the docked-vesicle intensity

Our procedure entailed measuring the docked-vesicle intensity, I_{dock}, for each fusion event and extracting the intensity reduction factor, λ_{TIRF}, by fitting our model to the fluorescence profile (Figs. 2 *C* and see 4 *A*). An important self-consistency check is that λ_{TIRF} is a unique function of I_{dock}, since the value of I_{dock} fixes the vesicle size and hence the value of λ_{TIRF} (Fig. 6 *A*). When we pooled the values for several compositions labeled with LE-PE and included nonspecific fusion events, the λ_{TIRF} -versus- I_{dock} data collapsed around a definite curve (Fig. 6 *B*). The R_{ves}-versus- I_{dock} data collapsed similarly (Fig. 6 *C*). Thus, our method satisfies this self-consistency check.

DISCUSSION

Single exocytotic fusion pores were first detected almost 30 years ago (50,51), shortly followed by observations of rapid flickering between the open and closed states (26,50). Neuroendocrine cells regulate hormone release by adapting the incidence and flickering dynamics of fusion pores to physiologic inputs (12). Pores also flicker during synaptic vesicle release, but the prevalence is less established, in part because of technical difficulties in probing pore properties during synaptic-vesicle exocytosis using direct electrical approaches. The few such measurements showed that 3–40% of pores flicker during synaptic-vesicle release (4,13) and that the flickering dynamics are regulated by phosphorylation (4). Possibly the most convincing data are from midbrain neurons that form "social" synapses and release dopamine that is sensed by receptors some distance (several micrometers) away from release sites (4). For such volume transmission, pore flickering would control the kinetics and spatial extent of receptor activation (4). In addition, "whispering" synapses at which downstream receptors are not activated may be associated with slow release through flickering fusion pores (15), and neurotransmitter release through transient pores may facilitate rapid recycling of synaptic vesicles (4).

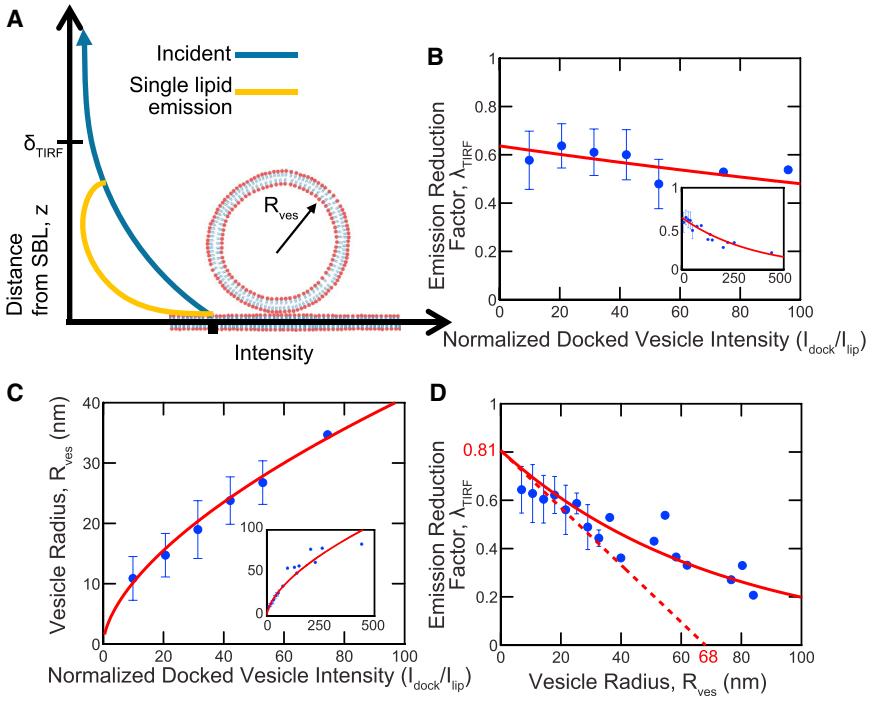

FIGURE 6 In TIRFM, the vesicle size and fluorescence reduction factor are unique functions of the docked-vesicle intensity. (*A*) The fluorescence intensity of a labeled lipid at a distance z from the SBL in a vesicle of radius R_{ves} (*lighter, yellow curve*) is the product of the decaying incident evanescent wave intensity (*darker, blue curve*) and a polarization factor due to lipid orientation. The net fluorescence reduction factor for the vesicle, λ_{TIRF}, is the average of the lighter yellow curve weighted by the number of lipids at each height. (*B* and *C*) λ_{TIRF} and R_{ves} are uniquely determined by the docked-vesicle intensity (139 fusion events; see the Supporting Material). (*B*) Values of λ_{TIRF} versus docked-vesicle intensity, I_{dock}, from this study follow a best-fit exponential $0.64\exp(-I_{dock}/350\,I_{lip})$ ($p < 0.05$) (*solid, red curve*). The bin size is 10.7. (*C*) Values of R_{ves} versus I_{dock} are well described by the best-fit power law $R_{ves} = 2.6\,(I_{dock}/I_{lip})^{0.61}$ nm ($p < 0.05$). The bin size is 10.7. (*D*) Values of λ_{TIRF} versus R_{ves} from this study. The tangent at the origin (*red dashed line*) is a linear fit to R_{ves}<35 nm points, constraining the intercept on the R_{ves} axis to be the TIRF decay length, $\delta_{TIRF} = 68$ nm (Supporting Material and Eq. S18) ($p < 0.05$). This yielded $\lambda^0_{TIRF} = 0.81$ for the limiting value of λ_{TIRF} for small vesicles, a pure polarization effect. The bin size 3.6 nm. In (*B*)–(*D*), values are shown as the mean (*dark, blue symbols*) ± SD. To see this figure in color, go online.

The underlying molecular mechanisms of fusion-pore flickering remain poorly understood. Here, we used TIRFM to study the dynamics of single SNARE-mediated fusion pores in vitro for the first time to our knowledge.

Most fusion pores reseal after slow release of lipids and soluble cargo

We simultaneously monitored soluble content marker SRB and lipid label DiD as single v-SUVs fused with t-SBLs, with ~18 ms time resolution. To within a single frame, release of the two types of label commenced simultaneously, and content release never preceded lipid release. After an initial release usually too slow to be compatible with a fully open, static pore, the pore resealed in >80% of all events, trapping some of the content labels. Our results suggest that the slow release was due to small, flickering pores. Consistent with this, using a vSUV-tSUV fusion assay, Lai et al. (52) suggested that an ~2-nm-diameter fusion pore retarded cargo release.

The size of a docked vesicle can be directly inferred from the docked-vesicle intensity in TIRFM

TIRFM is a powerful technique that selectively illuminates a small, ~100-nm-deep region adjacent to a substrate (29). Ideally, one would like to use the method to directly infer the size or location of illuminated objects from the fluorescence intensity, but this relation is not a priori known. For a docked spherical vesicle, the intensity results both from the decay of the evanescent field with distance from the substrate and from the varied orientations of labeled lipids at different locations in the vesicle whose fluorophores thus interact differently with the polarized illuminating field (Fig. 6 *A*).

Here, by tracking individual fusion events, we measured this characteristic relationship, which for a given TIRFM setup and lipid marker quantifies the relative contributions of evanescent wave decay and polarization effects to the normalized fluorescence intensity, λ_{TIRF}, as a function of vesicle radius (Fig. 6 *D*). It can be shown that the slope at the origin is $-\lambda^0_{TIRF}/\delta_{TIRF}$, where λ^0_{TIRF} is the value at zero radius and δ_{TIRF} the decay length of the evanescent excitation field, 68 nm here (see the Supporting Material). The best-fit tangent at the origin yielded $\lambda^0_{TIRF} = 0.81 \pm 0.03$, a pure polarization contribution for the label LR-PE, since evanescent field decay effects are absent as vesicle size tends to zero, and quenching effects are expected to be negligible as our lipid labeling densities are below the self-quenching threshold. λ^0_{TIRF} being less than unity shows that the evanescent field polarization (*s*-polarization here) is a worse match for labeled lipids in the vesicle, averaged over all lipid orientations in the spherical vesicle, than for lipids in the SBL.

Fusion pores mediated by SNARE proteins flicker rapidly

When vesicles fused with the SBL, vesicle-to-SBL lipid release rates were up to two orders of magnitude slower than they would be through fully open pores (Fig. S1 *C*). We conclude that pores flickered at rates $\gtrsim$ 100 Hz, the resolution limit of our measurements set by the time for a lipid to diffuse a distance of the order of the vesicle size, τ_{ves} ~ 10 ms. The small release rates could not be explained by permanently open but narrow pores, as this would require invoking pore radii, r_p, for lipid release less than the minimum value, ~2 nm, the lipid monolayer thickness. We remind the reader that our definition of the pore radius includes the inner monolayer (see Fig. S1 *A*, Eq. 1, and below). Thus, SNARE-mediated pores flicker rapidly in the absence of other fusion-machinery components.

Lipid membranes alone sustain flickering pores

We analyzed the population of slow nonspecific fusion events (32) and fusion events with protein-free SBLs, for both of which we assumed SNARE-independent fusion-pore dynamics. For all compositions but those with the highest cholesterol levels studied, pores flickered with statistics similar to those of SNARE-mediated pores: the flickering-pore openness, the fraction that were fully open, and the cholesterol dependence were similar (Fig. 4, *C* and *D*). This is consistent with previous observations of flickering pores in protein-free systems (53). This also provides further evidence that lipid diffusion is not severely restricted at the fusion pore by SNARE transmembrane domains. Our results suggest that in cells, a major component of the mechanism of fusion-pore flickering derives from the biophysical properties of the phospholipid membranes themselves, independent of SNAREs or other fusion machinery.

Cholesterol opens fusion pores by lowering the pore bending energy

Increasing amounts of cholesterol dramatically opened fusion pores (Fig. 4, *B–D*). At physiological cholesterol levels, flickering pores had a mean openness of P_o ~ 0.4, similar to the values $P_o \sim 0.3 - 0.8$ that we estimate for exocytotic pores from electrophysiological measurements (3,4,7,10). In addition, ~40% of pores were permanently open, suggesting that this may be true of exocytotic pores.

It follows that cholesterol lowers the free energy of pore formation, ΔF_{pore}, which is closely related to P_o. This trend was consistent for SNARE-mediated and SNARE-independent pores, suggesting that the origin lies in membrane energetics. Thus, adapting the model of (54), we calculated the change in the fusion-pore bending energy due to cholesterol, whose negative spontaneous curvature favors the net negative curvature of the fusion pore. Cholesterol lowered ΔF_{pore}, with a reduction of ~43 k_BT at physiological levels (Fig. S5), signifying essentially open pores, $P_o = 1$. These results can qualitatively explain the experimental trend; however, we observed that a significant fraction of pores remained flickering, suggesting additional effects beyond this simple model.

Cholesterol promotes fusion by direct membrane effects and by indirect promotion of SNARE-mediated fusion

We found that SNAREs play a very minor role in pore flickering when cholesterol is absent or at intermediate concentrations (Fig. 4, *C* and *D*), suggesting that cholesterol opens pores solely through its direct effect on membrane bending energy for these conditions. However at physiological cholesterol levels, SNAREs exerted a pronounced pore-opening effect as their presence increased the fraction of permanently open pores ~2-fold (Fig. 4 *D*). Moreover, at

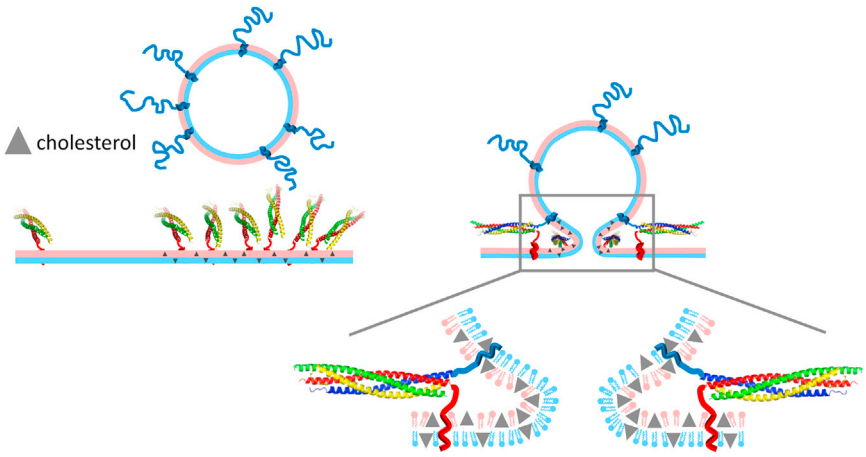

FIGURE 7 Model of promotion of SNARE-mediated fusion by cholesterol. Cholesterol (*triangles*) clusters t-SNAREs in target membranes (*left*), increasing vesicle docking rates and providing multiple t-SNAREs that are instantly available for accelerated fusion (*right*). Once initiated, the openness of the flickering pore is increased by cholesterol 1) directly, by lowering the bending energy of the pore (Fig. S5), whose negative curvature is compatible with cholesterol's large, negative spontaneous curvature, ~−0.4 nm^{-1} (55) (blow up, right); or 2) indirectly, by increasing the number of SNAREpins at the fusion pore. Increased openness stabilizes the pore and may increase content release rates and accelerate pore dilation (Fig. 1). To see this figure in color, go online.

these cholesterol levels, fusion occurred so rapidly after docking that there was insufficient time to recruit additional t-SNAREs, suggesting that t-SNAREs were preclustered at the docking site (Fig. 5 *A*), which is consistent with previous reports of cholesterol-mediated t-SNARE clustering (46–49).

A growing body of evidence suggests that cholesterol opens pores and augments fusion rates (20,23,24). Our results suggest that cholesterol facilitates exocytosis both directly, by lowering the energy to deform membranes into the severely bent shape of a fusion pore, and indirectly through its influence on SNARE proteins (Fig. 7). We propose that by clustering t-SNAREs in target membranes, cholesterol increases vesicle docking rates and increases the number of SNAREpins that cooperate to create and maintain a fusion pore, thereby increasing the openness of the pore (36). By increasing openness, these effects stabilize fusion pores, increase rates of content release, and may accelerate pore dilation.

SUPPORTING MATERIAL

Supporting Materials and Methods, Supporting Results, seven figures, and three tables are available at http://www.biophysj.org/biophysj/supplemental/S0006-3495(16)00165-X.

AUTHOR CONTRIBUTIONS

E.K. designed and performed the experiments. Z.W. and J.N. performed the single- and two-color experiments, respectively. B.O. performed the modeling analysis. B.O., B.S., and J.W. performed data analysis. B.S., G.W., E.W., and J.N. performed vesicle and lipid tracking, and Z.W. and E.K. performed vesicle tracking. D.B. designed the two-color-emission optical setup and helped E.K. to build it. D.B. and J.N. performed analysis of two-color images. B.O., B.S., and E.K. wrote the manuscript with input from others.

ACKNOWLEDGMENTS

We thank J. E. Rothman for providing equipment and lab space during the initial phase of this work and members of the O'Shaughnessy, Karatekin, and Rothman groups for helpful discussions. We thank Vladimir Polejaev (Yale West Campus Imaging Core) for building the polarized TIRF microscope used for the two-color experiments.

E.K. is supported by a Kavli Neuroscience Scholar Award from the Kavli Foundation and by National Institutes of Health grant 1R01GM108954.

SUPPORTING CITATIONS

Reference (56) is included in the Supporting Material.

REFERENCES

1. Lindau, M., and G. Alvarez de Toledo. 2003. The fusion pore. *Biochim. Biophys. Acta.* 1641:167–173.
2. Südhof, T. C., and J. E. Rothman. 2009. Membrane fusion: grappling with SNARE and SM proteins. *Science.* 323:474–477.
3. Zhou, Z., S. Misler, and R. H. Chow. 1996. Rapid fluctuations in transmitter release from single vesicles in bovine adrenal chromaffin cells. *Biophys. J.* 70:1543–1552.
4. Staal, R. G. W., E. V. Mosharov, and D. Sulzer. 2004. Dopamine neurons release transmitter via a flickering fusion pore. *Nat. Neurosci.* 7:341–346.
5. Bai, J., C. T. Wang, …, E. R. Chapman. 2004. Fusion pore dynamics are regulated by synaptotagmin*t-SNARE interactions. *Neuron.* 41:929–942.
6. Sombers, L. A., H. J. Hanchar, …, A. G. Ewing. 2004. The effects of vesicular volume on secretion through the fusion pore in exocytotic release from PC12 cells. *J. Neurosci.* 24:303–309.
7. Alvarez de Toledo, G., R. Fernández-Chacón, and J. M. Fernández. 1993. Release of secretory products during transient vesicle fusion. *Nature.* 363:554–558.
8. Han, X., C. T. Wang, …, M. B. Jackson. 2004. Transmembrane segments of syntaxin line the fusion pore of Ca^{2+}-triggered exocytosis. *Science.* 304:289–292.
9. Monck, J. R., and J. M. Fernandez. 1992. The exocytotic fusion pore. *J. Cell Biol.* 119:1395–1404.
10. Monck, J. R., G. Alvarez de Toledo, and J. M. Fernandez. 1990. Tension in secretory granule membranes causes extensive membrane transfer through the exocytotic fusion pore. *Proc. Natl. Acad. Sci. USA.* 87:7804–7808.
11. Breckenridge, L. J., and W. Almers. 1987. Final steps in exocytosis observed in a cell with giant secretory granules. *Proc. Natl. Acad. Sci. USA.* 84:1945–1949.
12. Fulop, T., S. Radabaugh, and C. Smith. 2005. Activity-dependent differential transmitter release in mouse adrenal chromaffin cells. *J. Neurosci.* 25:7324–7332.
13. He, L., X. S. Wu, …, L. G. Wu. 2006. Two modes of fusion pore opening revealed by cell-attached recordings at a synapse. *Nature.* 444:102–105.
14. Klyachko, V. A., and M. B. Jackson. 2002. Capacitance steps and fusion pores of small and large-dense-core vesicles in nerve terminals. *Nature.* 418:89–92.
15. Lisman, J. E., S. Raghavachari, and R. W. Tsien. 2007. The sequence of events that underlie quantal transmission at central glutamatergic synapses. *Nat. Rev. Neurosci.* 8:597–609.
16. Fang, Q., K. Berberian, …, M. Lindau. 2008. The role of the C terminus of the SNARE protein SNAP-25 in fusion pore opening and a model for fusion pore mechanics. *Proc. Natl. Acad. Sci. USA.* 105:15388–15392.
17. Breckenridge, W. C., G. Gombos, and I. G. Morgan. 1972. The lipid composition of adult rat brain synaptosomal plasma membranes. *Biochim. Biophys. Acta.* 266:695–707.
18. Takamori, S., M. Holt, …, R. Jahn. 2006. Molecular anatomy of a trafficking organelle. *Cell.* 127:831–846.
19. Traynor, A. E., D. Schubert, and W. R. Allen. 1982. Alterations of lipid metabolism in response to nerve growth factor. *J. Neurochem.* 39:1677–1683.
20. Linetti, A., A. Fratangeli, …, P. Rosa. 2010. Cholesterol reduction impairs exocytosis of synaptic vesicles. *J. Cell Sci.* 123:595–605.
21. Wang, N., C. Kwan, …, F. W. Tse. 2010. Influence of cholesterol on catecholamine release from the fusion pore of large dense core chromaffin granules. *J. Neurosci.* 30:3904–3911.
22. Zhang, Z., and M. B. Jackson. 2010. Membrane bending energy and fusion pore kinetics in Ca^{2+}-triggered exocytosis. *Biophys. J.* 98:2524–2534.
23. Tong, J., P. P. Borbat, …, Y. K. Shin. 2009. A scissors mechanism for stimulation of SNARE-mediated lipid mixing by cholesterol. *Proc. Natl. Acad. Sci. USA.* 106:5141–5146.
24. Biswas, S., S.-R. Yin, …, J. Zimmerberg. 2008. Cholesterol promotes hemifusion and pore widening in membrane fusion induced by influenza hemagglutinin. *J. Gen. Physiol.* 131:503–513.

25. Curran, M. J., F. S. Cohen, …, J. Zimmerberg. 1993. Exocytotic fusion pores exhibit semi-stable states. *J. Membr. Biol.* 133:61–75.

26. Spruce, A. E., L. J. Breckenridge, …, W. Almers. 1990. Properties of the fusion pore that forms during exocytosis of a mast cell secretory vesicle. *Neuron.* 4:643–654.

27. B. Sackmann, and E. Neher, editors 1995. Single-Channel Recording. Plenum Press, New York.

28. Chizmadzhev, Y. A., F. S. Cohen, …, J. Zimmerberg. 1995. Membrane mechanics can account for fusion pore dilation in stages. *Biophys. J.* 69:2489–2500.

29. Axelrod, D. 2008. Total internal reflection fluorescence microscopy. *Methods Cell Biol.* 89:169–221.

30. Cremona, O., and P. De Camilli. 2001. Phosphoinositides in membrane traffic at the synapse. *J. Cell Sci.* 114:1041–1052.

31. Karatekin, E., and J. E. Rothman. 2012. Fusion of single proteoliposomes with planar, cushioned bilayers in microfluidic flow cells. *Nat. Protoc.* 7:903–920.

32. Karatekin, E., J. Di Giovanni, …, J. E. Rothman. 2010. A fast, single-vesicle fusion assay mimics physiological SNARE requirements. *Proc. Natl. Acad. Sci. USA.* 107:3517–3521.

33. Kyoung, M., Y. Zhang, …, A. T. Brunger. 2013. Studying calcium-triggered vesicle fusion in a single vesicle-vesicle content and lipid-mixing system. *Nat. Protoc.* 8:1–16.

34. Hung, W.-C., M.-T. Lee, …, H. W. Huang. 2007. The condensing effect of cholesterol in lipid bilayers. *Biophys. J.* 92:3960–3967.

35. Smith, M. B., E. Karatekin, …, D. Vavylonis. 2011. Interactive, computer-assisted tracking of speckle trajectories in fluorescence microscopy: application to actin polymerization and membrane fusion. *Biophys. J.* 101:1794–1804.

36. Shi, L., Q. T. Shen, …, F. Pincet. 2012. SNARE proteins: one to fuse and three to keep the nascent fusion pore open. *Science.* 335:1355–1359.

37. Chernomordik, L. V., G. B. Melikyan, and Y. A. Chizmadzhev. 1987. Biomembrane fusion: a new concept derived from model studies using two interacting planar lipid bilayers. *Biochim. Biophys. Acta.* 906: 309–352.

38. Honigmann, A., G. van den Bogaart, …, R. Jahn. 2013. Phosphatidylinositol 4,5-bisphosphate clusters act as molecular beacons for vesicle recruitment. *Nat. Struct. Mol. Biol.* 20:679–686.

39. Liu, T., W. C. Tucker, …, J. C. Weisshaar. 2005. SNARE-driven, 25-millisecond vesicle fusion in vitro. *Biophys. J.* 89:2458–2472.

40. Durning, C., and B. O'Shaughnessy. 1988. Diffusion controlled reactions at an interface. *J. Chem. Phys.* 88:7117–7128.

41. Bowen, M. E., K. Weninger, …, S. Chu. 2004. Single molecule observation of liposome-bilayer fusion thermally induced by soluble *N*-ethyl maleimide sensitive-factor attachment protein receptors (SNAREs). *Biophys. J.* 87:3569–3584.

42. Zimmerberg, J., R. Blumenthal, …, S. J. Morris. 1994. Restricted movement of lipid and aqueous dyes through pores formed by influenza hemagglutinin during cell fusion. *J. Cell Biol.* 127:1885–1894.

43. Tse, F. W., A. Iwata, and W. Almers. 1993. Membrane flux through the pore formed by a fusogenic viral envelope protein during cell fusion. *J. Cell Biol.* 121:543–552.

44. Chen, Y. D., R. J. Rubin, and A. Szabo. 1993. Fluorescence dequenching kinetics of single cell-cell fusion complexes. *Biophys. J.* 65: 325–333.

45. Razinkov, V. I., G. B. Melikyan, and F. S. Cohen. 1999. Hemifusion between cells expressing hemagglutinin of influenza virus and planar membranes can precede the formation of fusion pores that subsequently fully enlarge. *Biophys. J.* 77:3144–3151.

46. Lang, T., D. Bruns, …, R. Jahn. 2001. SNAREs are concentrated in cholesterol-dependent clusters that define docking and fusion sites for exocytosis. *EMBO J.* 20:2202–2213.

47. Barg, S., M. K. Knowles, …, W. Almers. 2010. Syntaxin clusters assemble reversibly at sites of secretory granules in live cells. *Proc. Natl. Acad. Sci. USA.* 107:20804–20809.

48. van den Bogaart, G., K. Meyenberg, …, R. Jahn. 2011. Membrane protein sequestering by ionic protein-lipid interactions. *Nature.* 479: 552–555.

49. Milovanovic, D., A. Honigmann, …, R. Jahn. 2015. Hydrophobic mismatch sorts SNARE proteins into distinct membrane domains. *Nat. Commun.* 6:5984.

50. Breckenridge, L. J., and W. Almers. 1987. Currents through the fusion pore that forms during exocytosis of a secretory vesicle. *Nature.* 328:814–817.

51. Zimmerberg, J., M. Curran, …, M. Brodwick. 1987. Simultaneous electrical and optical measurements show that membrane fusion precedes secretory granule swelling during exocytosis of beige mouse mast cells. *Proc. Natl. Acad. Sci. USA.* 84:1585–1589.

52. Lai, Y., J. Diao, …, Y. K. Shin. 2013. Fusion pore formation and expansion induced by Ca^{2+} and synaptotagmin 1. *Proc. Natl. Acad. Sci. USA.* 110:1333–1338.

53. Chanturiya, A., L. V. Chernomordik, and J. Zimmerberg. 1997. Flickering fusion pores comparable with initial exocytotic pores occur in protein-free phospholipid bilayers. *Proc. Natl. Acad. Sci. USA.* 94: 14423–14428.

54. Kozlov, M. M., S. L. Leikin, …, Y. A. Chizmadzhev. 1989. Stalk mechanism of vesicle fusion. Intermixing of aqueous contents. *Eur. Biophys. J.* 17:121–129.

55. Chen, Z., and R. P. Rand. 1997. The influence of cholesterol on phospholipid membrane curvature and bending elasticity. *Biophys. J.* 73:267–276.

56. Wagner, M. L., and L. K. Tamm. 2001. Reconstituted syntaxin1a/SNAP25 interacts with negatively charged lipids as measured by lateral diffusion in planar supported bilayers. *Biophys. J.* 81:266–275.